JOTCS A
Journal of the Turkish Chemical Society
Section: A
Chemistry

TURKISH CHEMICAL SOCIETY

Accuracy Limits of Pair Distribution Function Analysis in Structural Characterization of Nanocrystalline Powders by X-ray Diffraction

Abolfazl Baloochiyan[1], Merdan Batyrow[1], Hande Öztürk[1*]

[1]Özyeğin University, Department of Mechanical Engineering, İstanbul, 34794, Turkey

Abstract: We report the minimum errors of structural parameters, namely lattice parameter, crystallite size, and atomic displacement parameters, expected from Pair Distribution Function (PDF) analysis of nanocrystalline gold powders for the first time by a self-consistent computational methodology. Although PDF analysis has been increasingly used to characterize nanocrystalline powders by X-rays, the current literature includes no established error bounds to be expected from the resulting structural parameters. For accurate interpretation of X-ray diffraction data, these error bounds must be determined, and the obtained structural parameters must be cleared from them. Our novel methodology includes: **1)** simulation of ideal powder diffraction experiments with the use of the Debye scattering equation, **2)** pair distribution function analysis of the diffraction data with the Diffpy-CMI analysis software, and **3)** determination of the errors from PDF analysis of the simulated diffraction data by comparing them with real-space analysis of spherical gold nanocrystals that are 30 nm size and smaller. Our results show that except for the lattice parameters and even with an ideal crystalline powder sample and ideal diffraction data, the extracted structural parameters from PDF analysis diverge from their true values for the studied nanopowder. These deviations are dependent on the average size of the nanocrystals and the energy of the X-rays selected for the diffraction experiments, where lower X-ray energies and small-sized nanocrystalline powders lead to greater errors.

Keywords: Pair distribution function analysis, powder diffraction, X-rays, nanocrystalline powders, Debye scattering equation.

Submitted: October 13, 2021. **Accepted:** March 13, 2022.

Cite this: Baloochiyan A, Batyrow M, Öztürk H. Accuracy Limits of Pair Distribution Function Analysis in Structural Characterization of Nanocrystalline Powders by X-ray Diffraction. JOTCSA. 2022;9(2):527–44.

DOI: https://doi.org/10.18596/jotcsa.1008896.

***Corresponding author:** hande.ozturk@ozyegin.edu.tr.

INTRODUCTION

Nanomaterials are becoming an integral part of all manufacturing processes in industries ranging from food, cosmetics, and weaponry, since they promise tunable physical, electrical, mechanical, etc. properties (1,2) that can potentially bring revolutionary solutions to many problems in engineering designs. The number one step for controlled manufacturing and/or integration of nanomaterials in mass production is fast, reliable, and robust characterization, which must be performed with the highest amount of detail and resolution to optimize nanomaterials for best performance. X-ray diffraction (XRD) is currently the gold standard characterization technique that promises these requirements while accessing atomic-scale information in a non-destructive manner (3). Although XRD was initially developed to investigate the atomic periodicity in crystalline materials, the technique has progressed enormously and has been extended to the analysis of amorphous materials as well. Among the most frequent practices of X-ray diffraction is powder diffraction. In this technique, one has no obligation to prepare high quality single crystalline samples, which is an obstacle for many materials (4), but can also investigate polycrystalline and powder forms of

materials as well. This has caught the attention of researchers working in the field of nanopowders, a class of nanomaterials consisting of nanocrystalline particles, and has resulted in further development of the XRD technique on nanoparticulate forms of matter.

In XRD analysis of nanopowders, there are mainly two methodologies one can follow: **1)** perform whole pattern modelling and refinement analysis assuming there is a unit cell model that represents the atomic ordering in the coherent domain of the material and work towards solving for that cell model from the diffraction data; or **2)** abandon the unit cell construct and perform modelling and refinement analysis of bond distance histograms of the coherent domains of the material by Fourier transforming the powder diffraction data (5). The first method is known as the structure solution methodology, and Rietveld refinement (6) is the most widely used algorithm in this context. The second method, known as the pair distribution function analysis, has been around for a while, but it has become popular with the development of open source computer programs (7) and the availability of synchrotron X-ray sources, enabling enormous progress in the capabilities of the technique.

For bulk crystalline materials where the atomic periodicity extends beyond hundreds of nanometers (8), crystallographic solutions are generally available from their diffraction data, and the resulting unit cell typically represents the average structural properties of the material. There is no guarantee that this solution is unique (9); however, one may complement X-ray analysis with independent, direct or indirect methods for confirmation, such as Transmission Electron Microscopy (TEM) or electrical conductivity, respectively. For nanocrystalline materials, crystallographic analysis is not as trivial as in bulk crystalline materials; in this case, atomic periodicity extends up to 100 nm or so, and thus typical diffraction data from such materials show structural features intermediate between those of crystalline and amorphous materials. There are certain regions in nanomaterials where the atomic stacking can be described as periodic, as in a regular crystal, and some other regions where this stacking cannot be considered periodic at all (10). For such materials, the assumption of a single unit cell representing the average atomic configuration within the material is unjustified (11). Therefore data analysis methods relying on the assumption of a unit cell model fail. In that case, pair distribution function analysis, assuming no particular atomic stacking within the scattering material and no single repeating unit cell, may be the right solution for structural analysis of nanocrystalline powders and is quickly becoming popular.

In an earlier work, we demonstrated that widespread crystallographic analysis routines, such as line profile analysis and Rietveld refinement, failed to retrieve the true lattice parameters of nanocrystalline powders (11) and identified the reason for failure as the incompatible single unit cell model used to represent the atomic configuration of atoms in nanocrystals. In the current work, we implement our self-consistent methodology to quantify the minimum errors within the structural parameters, i.e., lattice parameters, average crystallite sizes, and atomic displacement parameters, retrieved from pair distribution function analysis and evaluate how errors vary with respect to the energy of the X-rays and the average size of the nanocrystals studied. Our findings will potentially guide researchers working on the characterization of nanomaterials to use pair distribution function analysis properly with realistic expectations for accuracy, interpret their results correctly, and design their experimental setups better for improved accuracy in structural identification of nanocrystalline powders.

THEORY

A typical PDF experiment consists of: **1)** measuring the coherent X-ray scattering intensity $I_{coh}(q)$ from an ensemble of atoms in the kinematic scattering regime; **2)** manipulating this measurement to extract what is called the normalized total scattering function S(q); **3)** a Fourier transformation to convert the total scattering function to another function of real space, r, that is an indirect representation of distances between pairs of atoms making up the crystal (5). This resulting transform is called the reduced pair distribution function G(r), and it is then refined to extract structural parameters of the irradiated sample. These steps can be mathematically formulated as below:

$$I_{coh}(q)=\sum_{i=1}^{N}\sum_{j=1}^{N} f_i f_j exp\left(iq.\left[r_i-r_j\right]\right) \quad \text{(Eq.1)}$$

where N is the number of atoms that are irradiated by X-rays, $f=f(q)$ is the atomic scattering factor of the type of material which depends on the scattering angle 2θ and the irradiation wavelength, λ, r_i is the coordinate vector of the atom i from an arbitrary origin and i is the imaginary number, $\sqrt{-1}$. A normalization is applied on I_{coh} to access the reduced total scattering function S(q):

$$S(q)-1=\frac{I_{coh}(q)}{N\langle f\rangle^2-\frac{f^2}{\langle f\rangle^2}} \quad \text{(Eq. 2)}$$

Where q is the magnitude of the momentum transfer vector of the X-rays, with

$q=|q|=\frac{4\pi \sin\theta}{\lambda}$ and $\langle f\rangle^2$ is the squared average atomic scattering factor. In Eq. 2, we highlight the term 'coherent intensity' to emphasize that the reduced total scattering function is related only to the coherent portion of measured X-ray intensities, hence -if applicable- the measured diffraction data must be cleared from unwanted signal such as that resulting from multiple scattering, sample absorption, background scattering, etc. Once S(q) is evaluated, the pair distribution function G(r) can be obtained by the following Fourier-Sine transform:

$$G(r)=\frac{2}{\pi}\int_0^{\infty} q\left[S(q)-1\right]\sin(qr)\,dq \qquad \text{(Eq.3)}$$

As can be seen, the reduced pair distribution function G(r) is theoretically accessible exactly from the measured coherent diffraction intensities by a standard normalization followed by a Fourier transform. But during real measurements, the upper limit of the integral in Eq. 3 is never infinite and is limited by the maximum scattering angle at which the diffraction intensities are recorded and the wavelength of X-rays. Accordingly, a truncated approximation of the Fourier-Sine transform is employed to obtain the reduced pair distribution function:

$$G(r)=\frac{2}{\pi}\int_{q_{min}}^{q_{max}} q\left[S(q)-1\right]\sin(qr)\,dq \qquad \text{(Eq. 4)}$$

where $q_{max}=\frac{4\pi\sin(\theta_{max})}{\lambda}$. This truncation is known to decrease the resolution of the real space function obtained from the Fourier transform (12). Similarly, the small angle scattering portion of the diffraction data is usually cropped, since diffraction intensities close to forward-scattering angles scale with the square of the total number of irradiated atoms and have the potential to burn the center of X-ray detectors due to extremely high photon counts, unless properly blocked. Secondly, including the small angle scattering portion in diffraction data results in an incompatibility with the expected input of the subsequent refinement process (13). Therefore, the small angle scattering portion is excluded from the integration, i.e., $q_{min}=\frac{4\pi\sin\theta_{min}}{\lambda}$ and $\theta_{min}>0$.

G(r) can also be evaluated using sample's real-space parameters. This can be accomplished by realizing that G(r) is actually the local deviation of the number density of atom pairs from the average number density of irradiated atoms separated by a particular interatomic distance r. Using this definition, G(r) can also be written as:

$$G(r)=\frac{1}{r}\sum_i^N\sum_j^N\left[\frac{f_i f_j}{\langle f\rangle^2}\delta(r-r_{ij})\right]-4\pi\rho_0 \qquad \text{(Eq. 5)}$$

where δ(r) is the Dirac delta function, $r_{ij}=|r_i-r_j|$ and ρ_0 is the average number density of the atomic ensemble. For an ensemble of atoms that are stacked perfectly periodic in 3 dimensions, like an ideal crystalline particle, Eq. 5 results in sharp and discrete Dirac delta functions, located at interatomic distances corresponding to characteristic interplanar distances of the crystallite. However, for all realistic crystalline and amorphous material samples measured at finite temperatures, the resulting thermal movement of atoms causes these Dirac delta functions to broaden, proportional to the amount of atomic displacement. Assuming random displacements of atoms around their average positions, each pair distribution peak can be numerically approximated by a Gaussian function. Hence, the width of these Gaussian functions can be used as a measure of the average displacements of atoms around their average positions, which can then be related to the Debye-Waller factor in X-ray diffraction experiments (5).

In conclusion, the main logic behind Pair Distribution Function refinement is to calculate a model G(r) based on the initial atomic coordinates assumed for the diffracting sample (using Eq. 5) and refine this model against the G(r) obtained from the diffraction signature of that sample (using Eqs. 2 and 4) until a predefined tolerance level is achieved between the two G(r) functions. Unlike standard Rietveld refinement analysis commonly used in crystallographic studies of polycrystalline, single crystalline, and nanocrystalline materials, the PDF refinement is based on a least square error minimization process performed on *real-space data*, rather than reciprocal (or angular, 2θ) space.

METHODOLOGY

Here we describe the four main steps followed to study the accuracy limits of the structural parameters obtained from gold nanocrystalline powders using their X-ray diffraction data. These are: **1)** creating the atomic coordinates of a nanocrystalline particle and generating an ideal, monodispersed particle ensemble from it; **2)** calculating the expected powder diffraction data from this nanocrystalline particle ensemble; **3)** steps followed during preprocessing of the diffraction data; and **4)** pair distribution function analysis.

Creating Perfectly-Crystalline and Energy-Minimized Versions of Ideally Random, Monodispersed Nanocrystalline Powders

This step includes creating atomic coordinates of spherical gold nanocrystals with two versions: ideal nanocrystalline and energy minimized atomic configurations. For ideal crystalline nanoparticles, we assumed a lattice parameter of 4.0626 Å and created atomic coordinates in 3 dimensions by following the packing rules of face centered cubic

crystals. Spherical nanocrystals with variable diameters were generated. For energy-minimized nanocrystals, we used these ideal-crystalline atomic configurations as input and performed equilibrium molecular dynamics (EMD) simulations assuming a 0 Kelvin final temperature. EMD simulations were performed with the open-source LAMMPS code (14) combining the initial (ideal-crystalline) atomic coordinates with interatomic forces modeled by the optimized embedded atom method (EAM) for gold atoms as suggested in the literature (15). These new coordinates were validated against similar work from past literature (11). Figure 1 shows the energy minimization process and the resulting atomic coordinates of ideal-crystalline and energy-minimized versions of a spherical gold nanoparticle with a 5 nm nominal diameter.

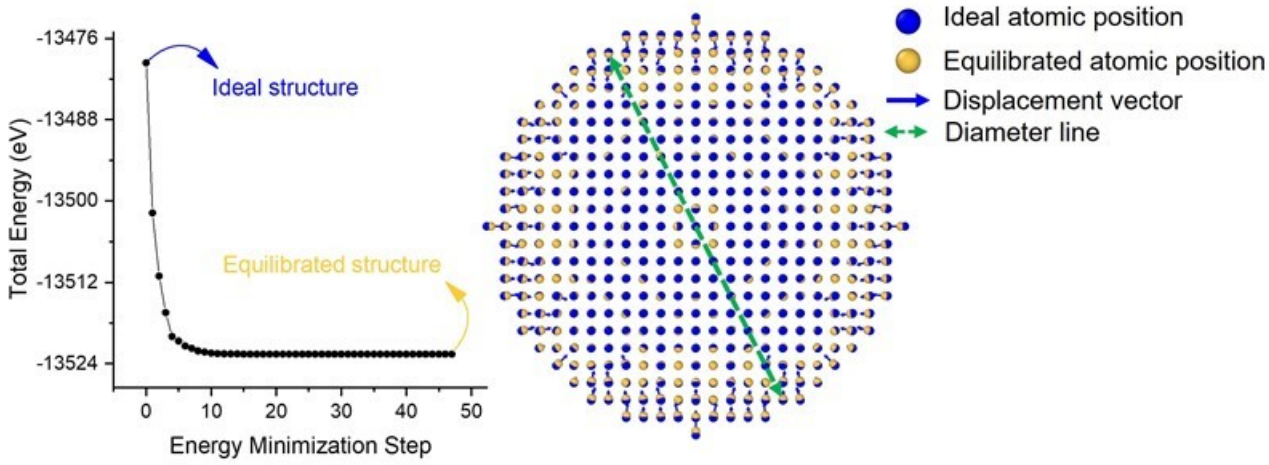

Figure 1: Left side: Change in the total energy of the spherical gold nanoparticle system during EMD simulations performed on ideal crystalline atomic configuration. The resulting energy-minimized atomic configuration has less total energy and is thermodynamically stable. The number of steps taken during the simulation was determined by the tolerance value of 10^{-8}. **Right side:** The atomic configurations of ideal-crystalline (blue markers) and energy-minimized versions (yellow markers) of the gold nanoparticle with a 5 nm nominal diameter. The blue arrows associated with blue markers show the relative displacement of atomic sites resulting from energy minimization. The green arrow drawn by dashed lines is one of the diameter lines we used to calculate the average size of the nanoparticle.

Once the atomic coordinates of a single gold nanoparticle are generated, we can create a monodispersed, ideal powder ensemble by considering a finite number of such particles and randomizing their orientation with respect to each other. The final set of atomic coordinates would constitute an ideal particle ensemble (powder) with a finite number of identical nanoparticles having random distribution of particle orientations. The diffracted intensities from such a finite particle ensemble would fluctuate around a mean value where the uncertainty in the intensities is inversely proportional to the number of particles considered (16). However, if we take the limit of the number of particles to infinity, then the orientationally-averaged diffracted X-ray intensities from these particles correspond to their ultimate limit with no statistical uncertainty. In this study, we focused on the accuracy limits of an X-ray analysis algorithm; hence, we chose to work with infinite-particle ensembles, eliminating statistical fluctuations in the diffraction data resulting from particle selection statistics.

Generation of Ideal Diffraction Profiles

The expected diffraction intensity distribution from infinitely large powders of gold nanocrystals was computed by the Debye scattering equation (17). This equation has the following form:

$$\langle I(2\theta)\rangle = f_m(2\theta) f_n(2\theta) \sum_{m=1}^{N} \sum_{n=1}^{N} \frac{\sin\left(|q||r_{mn}|\right)}{|q||r_{mn}|} \quad \text{(Eq. 6)}$$

Here $\langle I(2\theta)\rangle$ is the orientationally-averaged diffracted intensity distribution that is a function of the scattering angle 2θ, $|q|$ is the magnitude of the momentum transfer vector, $|r_{mn}| = |r_m - r_n|$ is the magnitude of the separation vector between atoms m and n, and $f_m(2\theta)$ is the atomic scattering factor of atom m, which is again angle dependent as q and is determined by the type of scattering material. For a monatomic crystal such as a gold nanoparticle, $f_m = f_n$; hence, $f_m(2\theta)f_n(2\theta) = f^2(2\theta)$. Finally, the upper limit of the summation N is the total number of atoms within a single nanoparticle. As seen from Eq. 6, one needs only the atomic coordinates of a single nanoparticle to generate the orientational average of the diffracted intensity distribution from a monodispersed ensemble of nanocrystals irradiated by monochromatic X-rays. This means that the Debye equation implicitly assumes that the

orientation distribution of nanocrystals making up the particle ensemble is ideally random, which also necessitates that the ensemble consists of an infinite number of identical crystals. Interested readers can follow classical texts (18) to confirm these assumptions behind the Debye equation.

To sum up, the Debye equation provides us with a powerful tool to test error bounds and applicability of X-ray analysis algorithms on diffraction data from nanocrystals, since we can work with noise-free, ideal diffraction data and have full control over the inputs to these algorithms.

In this study, the diffracted intensity data were obtained by the Debyer software[1], since coding Eq. 6 and directly running simulations with nanocrystals with large number of atoms N causes the computation time to explode quickly. This software optimizes the computation time neatly by generating histograms of available interatomic distance vectors, r_{mn} for each atom in the particle and considering only those terms that contribute appreciably to the diffracted intensities. Hence, it diverges slightly from the exact computation of the Debye equation. However, we confirmed that these deviations are minor, and do not affect our results, similar to past work (11). Next, we set the angular range as $2\theta \epsilon (5^{\circ}, 180^{\circ})$, angular spacing as $d\theta = 0.01^{\circ}$ and selected 5 different X-ray wavelengths from 0.21 to 1.54 Å, which are widely used in experimental studies[2]. Five different particle diameters were considered when modelling the nanocrystalline powders, which ranged from 5 to 30 nm. This process resulted in 50 different X-ray diffraction data since we considered both ideal crystalline and energy-minimized versions of these 5 nanocrystalline particle ensembles. Examples of computed diffraction data are seen on the left side of Figure 2. Finally, we emphasize that these intensities do not contain any unwanted scattering signals or background other than the coherent, elastic scattering from gold atoms. Hence, they were used directly in the subsequent analysis steps. When working with experimental diffraction data, one needs to carefully clean up their data from inelastic scattering, refraction effects, counting and particle selection statistics, and systematic/human errors, if present, before further analysis (12).

Preprocessing of Diffraction Data

Before performing the pair distribution function analysis, one should process the powder diffraction data. Typically, this process entails obtaining the normalized total scattering function S(q) from the intensity data and then performing the Fourier-Sine transform of the data. In this work, we performed these steps using the pdfgetx3 code (19), which is part of the Diffpy-CMI package (7) due to the software's being widely used by the X-ray community in PDF analysis.

An important step while performing the Fourier-Sine transform of the intensity data is the proper removal of the small angle scattering component. This was done by visualizing our simulated diffraction data one by one and setting an angular threshold below which there would be considered a small angle scattering component of the diffracted signal. This region was determined separately for each wavelength considered and reported in the last column of Table 1 as $q_{min} = \frac{4\pi \sin\theta_{min}}{\lambda}$. Finally, the default setting of r_{poly}=0.9 was used, since the minimum interatomic distance in our gold nanocrystals is around 2.872 Å, which is imposed by the stacking rules of the FCC unit cell, and r_{poly}=0.9 is not expected to affect our interatomic distances as explained by past literature (19). On the right side of Figure 2, examples of reduced pair distribution functions G(r) resulting from preprocessing of diffraction profiles of 5, 10, and 15 nm spherical gold nanoparticles are shown.

Pair Distribution Function Analysis and Refinement

After the intensity data are transformed, the final step is the PDF refinement. We used the freely-available module Diffpy-cmi (7) to perform our refinements. At the beginning of a refinement, one needs to provide the transformed intensity files as well as a cif file (crystallographic information file) of the powder material as input. This cif file, which in our case is the one for gold, is used to initialize the structural parameters such as lattice parameter, thermal parameters, etc., to be refined. Then, the real space range over which the refinement will be performed is selected, and the parameters are refined one-by-one. Typical refinement parameters are: **1)** an arbitrary scaling factor used to match the nominal values of the calculated and modeled pair distribution functions; **2)** average lattice parameter; **3)** coherent particle size, which is a measure of the average extent of atomic periodicity for diffracting particles; **4)** a damping factor q_{damp} used to quantify and implement the limited instrument resolution effects, such as X-ray wavelength and limited angular range of the X-ray detector, on the corresponding pair distribution function model; and **5)** thermal parameters such as Anisotropic Displacement Parameters (ADP) used to quantify static or dynamic, direction-dependent or independent, mean-squared atomic displacements from ideal lattice positions (20). During the refinement, the software tries to modify and match the modeled pair distribution function against that obtained from the Fourier Sine transform by a least-square optimization routine.

1 https://debyer.readthedocs.io/en/latest/

2 For simulations with λ=0.21Å, dθ = 0.001° and $2\theta \epsilon (0.1^{\circ}, 55^{\circ})$ since dθ > 0.001° was not narrow enough to resolve neighboring Bragg peaks clearly.

In this work, we started off by initializing the lattice parameter as 4.078 Å, crystal space group as Fm3m, B_{iso} as 0.001, a negligible but finite value to avoid crashing of the software since B_{iso}=0 corresponds to a case with Dirac delta functions as reduced pair distribution peaks, and instrument-related damping factor q_{damp} as 0.001, which is the default value assumed in Diffpy-cmi software, since our simulated data cannot be corrected against the refinement of a calibration material, unlike what is suggested in the literature (21). Next, we divided the whole refinement process into multiple steps; we refined the lattice parameter and the arbitrary scaling factor first, the coherent particle size, assuming spherical particle shapes second, B_{iso}, i.e. the atomic displacement parameter, assuming isotropic displacement of atoms, third, and then all parameters were refined altogether last. The quality of the refinement was confirmed by two measures: Rw, which is a goodness-of-fit parameter reported by the software, and by visual inspection of the calculated and measured pair distribution functions. We observed that relying solely on Rw was misleading since there is no universally accepted reference value for Rw for a particular fit quality.

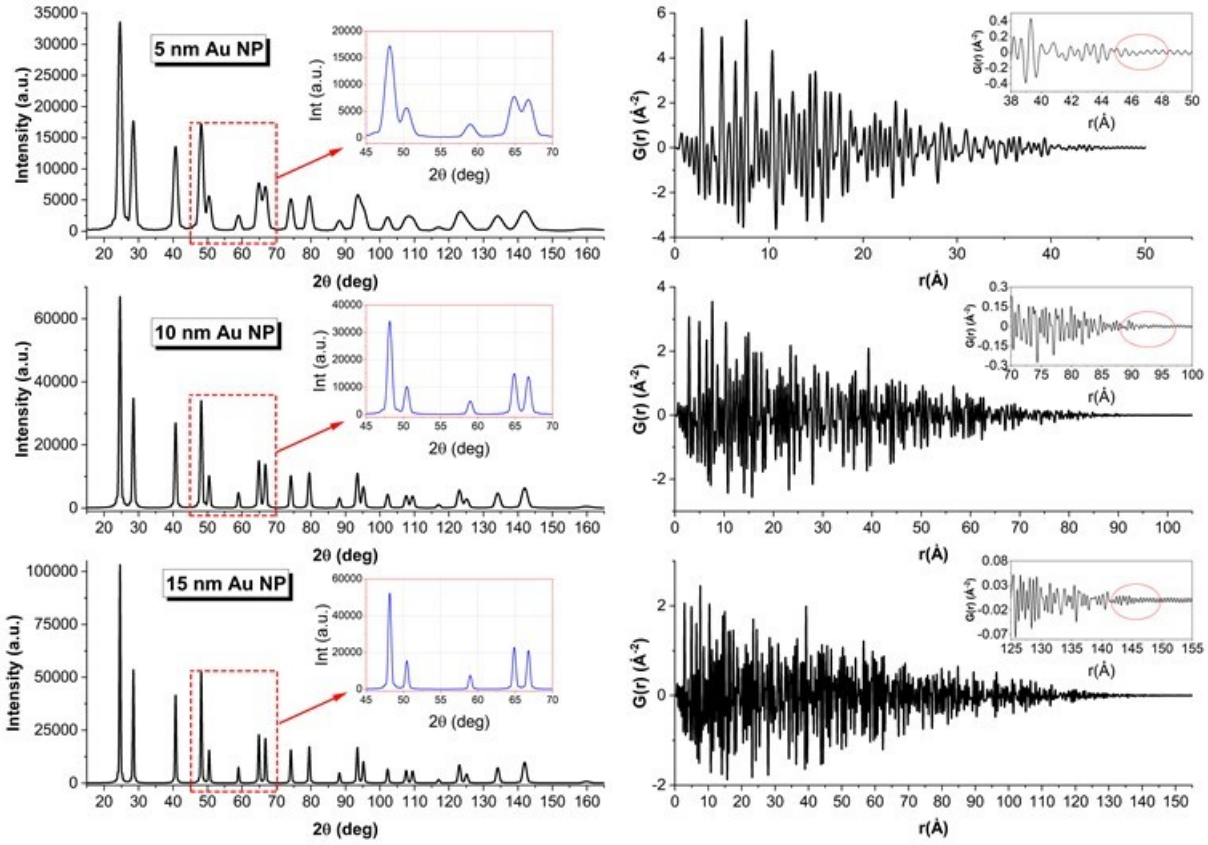

Figure 2: Left side: The simulated powder diffraction profiles of 5 nm (top), 10 nm (middle), 15 nm (bottom) diameter spherical gold nanoparticles assuming 1 Å wavelength X-rays. The insets show a close up view of the intensity distributions between 45° and 70°. **Right side:** The corresponding reduced pair distribution functions G(r) of the diffraction profiles on the left. The insets are a close up view of the tails where G(r) approaches background level.

RESULTS AND DISCUSSION

In this section, we report the outcomes of the pair distribution function analysis of diffraction data simulated from ideal, random, and monodispersed gold nanocrystals of various sizes and both in ideal crystalline and energy-minimized forms.

PDF Refinement of Diffraction Data from Ideal Crystalline Gold Nanopowders

An example of a successful PDF refinement is presented in Figure 3. Here, the diffraction data was simulated based on an ideal ensemble of 5 nm diameter, ideal-crystalline spherical gold nanoparticles, and 1 Å wavelength of X-rays. The left and right sides of the figure show, respectively, the full (0-60 Å) and short range (1.5-20 Å) portions of the reduced pair distribution function, obtained from the diffraction data itself (G_{obs} shown by black squares) and the best fitting model (G_{fit} shown by red curves) obtained by the refinement process. Blue curves at the bottom of the graphs are residuals, G_{obs}-G_{fit}, that quantify the difference between observed data and the fitted model. The

full-range refinement plot demonstrates that, overall, the positions and relative intensities of the reduced pair distribution function were captured correctly. The correct positioning of the fit centers can be confirmed from the short-range refinement plot as well: here the $G_{fit}(r)$ peaks with major intensities belong to the relative number of interatomic distances with lengths equal to peak center positions. For an ideal FCC gold crystallite with lattice parameter of 4.0626 Å, we can confirm that the first few interatomic distances available are 2.873, 4.063, 5.745 Å etc., which are the first, second, and third nearest interatomic distances in the cell. These are also the positions of the first three G(r) peaks, with the exception of the second peak, which shifted slightly off from its ideal position, i.e., 4.063 Å. The reason behind the shift here is an overlapping neighboring peak centered around 4.30 Å, which is not an actual G(r) peak but a Fourier truncation peak resulting from the limited q_{max} range of the intensity data (12). Finally, the full-range fit shows that the G(r) functions decay decrease to a noise level between 40 and 50 Å. This is an indication that no atom pair exists with a separation distance larger than these limits. The exact value of this distance is determined by a shape form factor that is implemented in the Diffpy-cmi algorithm (22) and is interpreted as the size of the coherent particle domain. For an ideal crystalline particle, the coherent domain size equals the average diameter of the particle.

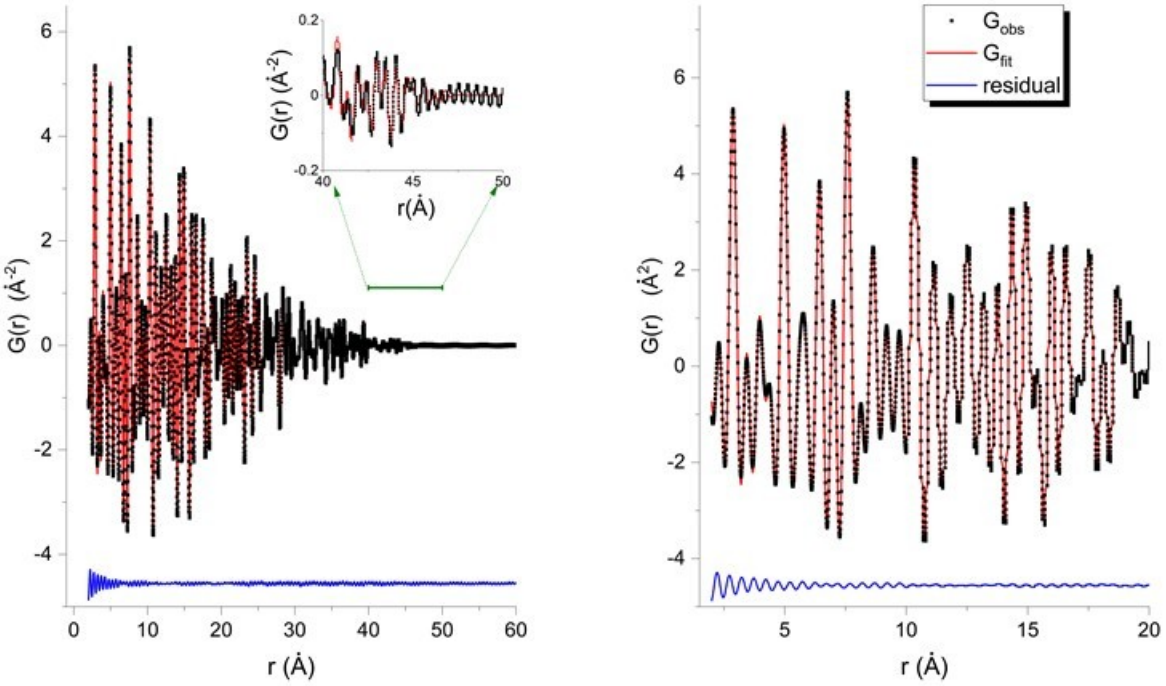

Figure 3: Left: Long range results of successful refinement of the diffraction data from 5 nm diameter ideal gold nanoparticles. The data was generated assuming 1 Å X-ray wavelength. The inset shows the tail of the fit for the real space interval of 40-50 Å. **Right:** Short range portion of the PDF analysis for the real space interval of 1.5-20 Å. The blue curve reports the residual between the observed G(r) function and the fitted model.

Table 1 presents the systematic PDF refinement results performed on the diffraction data of ideal crystalline nanoparticle ensembles with variable particle sizes irradiated at 5 different wavelengths. Here, nominal size is the intended diameter of the nanocrystals making up the ideal powders, λ is the assumed wavelength of the X-rays while computing the diffraction data, a is the refined lattice parameter, D is the refined particle diameter assuming spherical crystallites, q_{damp} and B_{iso} are the refined damping and isotropic atomic displacement factors of the modeled pair distribution function, respectively, $\Delta r = \frac{2\pi}{q_{max}}$ is the achievable real-space resolution of the processed diffraction data and finally, q_{min} and q_{max} are the minimum and maximum magnitudes of the momentum transfer vector allowed in the Fourier-Sine transform.

Table 1: PDF refinement results of diffraction data computed from ideal crystalline, spherical gold nanoparticle ensembles evaluated at 5 different wavelengths.

Nominal Size (Å)	λ (Å)	a (Å)	D (Å)	B_{iso} (Å²)	Rw	Δr (Å)	q_{min} (1/Å)	q_{max} (1/Å)
48.75	0.21	4.06263	48.74	0.002	0.043	0.10	1.56	27.6
97.50	0.21	4.06261	97.64	0.001	0.028	0.10	1.56	27.6
150	0.21	4.06260	150.55	0.001	0.025	0.10	1.56	27.6
195	0.21	4.06260	195.45	0.001	0.019	0.10	1.56	27.6
293	0.21	4.06260	293.97	0.002	0.016	0.10	1.56	27.6
48.75	0.56	4.06260	48.81	0.006	0.053	0.28	1.56	22.4
97.50	0.56	4.06260	97.46	0.002	0.018	0.28	1.56	22.4
150	0.56	4.06260	150.54	0.002	0.017	0.28	1.56	22.4
195	0.56	4.06260	195.30	0.002	0.013	0.28	1.56	22.4
293	0.56	4.06260	293.51	0.002	0.011	0.28	1.56	22.4
48.75	0.71	4.06255	49.07	0.011	0.055	0.35	1.54	17.7
97.50	0.71	4.06258	97.78	0.006	0.044	0.35	1.54	17.7
150	0.71	4.06260	150.88	0.003	0.032	0.35	1.54	17.7
195	0.71	4.06260	195.68	0.002	0.028	0.35	1.54	17.7
293	0.71	4.06260	294.01	0.002	0.023	0.35	1.54	17.7
48.75	1.00	4.06249	48.82	0.013	0.035	0.50	1.64	12.6
97.50	1.00	4.06259	97.76	0.009	0.027	0.50	1.64	12.6
150	1.00	4.06260	150.78	0.002	0.024	0.50	1.64	12.6
195	1.00	4.06260	195.62	0.005	0.019	0.50	1.64	12.6
293	1.00	4.06264	294.07	0.004	0.015	0.50	1.64	12.6
48.75	1.54	4.06264	48.98	0.001	0.050	0.77	1.70	8.2
97.50	1.54	4.06262	97.83	0.001	0.033	0.77	1.70	8.2
150	1.54	4.06261	150.79	0.001	0.027	0.77	1.70	8.2
195	1.54	4.06261	195.67	0.002	0.023	0.77	1.70	8.2
293	1.54	4.06260	294.17	0.002	0.020	0.77	1.70	8.2

As can be seen, the refined lattice parameters agree well with the assumed lattice parameter (a=4.0626 Å) during generation of the atomic coordinates of the ideal crystalline spherical gold nanoparticles for all particle sizes considered and at all X-ray wavelengths. They fluctuate only at the fifth decimal, which is in fact outside the accuracy limits of the lattice parameter that can be obtained from our diffraction data due to our angular spacing being set as $d\theta = 0.01^{o}$ and also the resolution of the pair distribution function analysis Δr >> 10^{-5} Å. Therefore, we can interpret these small fluctuations as resulting from numerical errors during the refinement process. When we look at the extracted diameters, we again see that they agree with the nominal particle diameters within 1% accuracy. There are two sources of error resulting in these small inaccuracies: the first one is the limited range of the q_{max} that approximates the Fourier Sine integral in Eq. 3 with a finite integration range, and the second one is the nominal particle shapes being far from ideal spheres. As explained in previous sections, ideal crystalline particles were obtained by carving out spheroidal shapes from an ideal 3D face-centered cubic lattice without considering the integrity of individual unit cells within the outer layers of the particle. Hence, these discrete spherical particles are actually spheroids with faceted surfaces (see Figure 1). The diameters of these shapes, therefore, are best expressed as a distribution of diameters around a mean value rather than an ideal Dirac delta function, and the width of this distribution adds to the inaccuracies in the extracted diameters from the PDF analysis. Nevertheless, the lattice parameters and the average crystallite diameters are obtained quite nicely, and even with limited resolution of reduced pair distribution functions with q_{max} as low as 8.2 $Å^{-1}$ (12). Such high performances from PDF analysis are impossible to achieve with experimentally-obtained diffraction data from real nanocrystalline samples. Therefore these accuracy limits must be interpreted as the best-case-scenario or equivalently, the minimum errors to be expected from the capabilities of PDF analysis.

When we look at how the PDF-extracted structural parameters compare with their true values at different wavelengths of X-rays, we notice that the most sensitive parameter to the X-ray energy and particle size is the isotropic atomic displacement factor, B_{iso}. This is a correction factor used when analyzing powder diffraction data and quantifies how much of an intensity decay should be expected in the diffraction data of an irradiated powder due to the amplitude of thermal vibrations of its constituent atoms. Because these vibration amplitudes cause lattice points to become finite volumes rather than being dimensionless points in 3D space, an increase in the temperature of an irradiated sample must cause a decreased probability of constructive

interference between atomic planes since their ideal periodicity is eventually lost. This effect has been studied in past literature, and it was concluded that these thermal vibrations of atoms do not cause any broadening in the corresponding Bragg peaks of the diffraction data, but only suppress their intensities, with an uneven and larger influence on higher order reflections (23). Their effect on the reduced pair distribution peaks is a broadening, which is typically modeled by a convolution operation of the G(r) peaks with a Gaussian function if the atomic vibrations are isotropic in all directions (12). Looking at Table 1, it can be seen that extracted B_{iso} values of all nanocrystal sizes vary between 0.001 and 0.013 $Å^2$. Although these non-zero atomic displacement parameters indicate the presence of atomic vibrations when there are none, they may result from numerical errors and the finite angular range of the diffraction data causing truncation errors in the Fourier transform since they are obtained from the PDF analysis of diffraction data computed from ideal nanocrystals where all constituent atoms are fixed at their lattice points (B_{iso} = 0). Finally, these erroneous B_{iso} values are generally higher for smaller particles than larger ones.

PDF refinement of diffraction data from energy-minimized Gold nanopowders

Table 2 presents our PDF refinement results of diffraction data simulated with energy-minimized versions of gold nanopowders considered previously. The difference here is that the atoms now experience finite displacements from their ideal lattice positions, since at 0 Kelvin temperature, the minimum-energy configurations of nanocrystalline particles do not necessarily correspond with those of an ideal FCC lattice, especially for surface-layer atoms as demonstrated in previous literature (11, 24). The static (time-independent) component of these displacements from the ideal lattice points are treated as microstrains in X-ray literature, and past work (25) showed that these microstrains were of compressive type at the nanoparticle surface, gradually decaying to a displacement-free core region of the nanoparticles, as seen in Figure 1. During PDF refinement, microstrain information was not extracted because there was no long-range atomic order assumed while refining for the modeled G(r) functions. Instead, all atomic displacements are treated as contributions to B_{iso}, irrespective of whether they result from static or dynamic displacements caused by temperature-dependent atomic vibrations[3] (20).

The findings in Table 2 confirm the inward movement of surface atoms as a result of the energy-minimization operation. As seen, for all wavelengths considered, the refined lattice parameters decrease with decreasing particle size. This can be explained by smaller nanocrystals experiencing much higher numbers of atomic displacements since they have a much higher proportion of their atoms on their surface layers compared to larger nanocrystals. These surface atoms are not fully coordinated with neighbor atoms as opposed to core atoms, so they can move more freely than core atoms. Hence, large amounts of inward displacement experienced by surface atoms cause a decrease in the average unit cell dimensions. With decreasing surface atom proportions in larger particles, the effect was less significant. Eventually, the lattice parameters of larger nanocrystals, such as those of 20 and 30 nm nominal diameters, are almost comparable to the initial lattice parameter of the particles, i.e. 4.0626 Å. This effect was confirmed in an earlier study as well (11) and is also visualized on the left side of Figure 3.

When looking at the extracted particle sizes, the indirect effect of the compressive strains on the nanoparticle surfaces can be noted. For all considered wavelengths, the refined diameters of energy-minimized nanoparticles are smaller than their ideal-crystalline counterparts. These differences are maximized for PDF refinement studies performed on the diffraction data computed with the smallest X-ray wavelengths (λ = 0.21 Å) than larger ones, as shown in the middle portion of Figure 4. The reason behind this wavelength-dependence is that the smallest wavelength enables the largest q_{max} range in the diffraction data and, correspondingly, the highest real-space resolution Δr and the minimum number of Fourier truncation errors. Therefore, the higher sensitivity in real-space enables the visibility of these small size differences. In addition, the reduction in the extracted diameters is bounded by the smallest nanocrystals (≈ 10%) on the upper limit, and the largest nanocrystals on the lower limit (≈ 2%), for all wavelengths studied. This is consistent with the different surface atom proportions of small and large nanocrystals and their resulting effects on the energy-minimization process.

3 As it can be noted, this treatment is inconsistent with the methodology followed in refinement methods based on structural solutions, such as Rietveld refinement, since the latter allows one to distinguish between microstrain and isotropic/anisotropic atomic displacements and extract both.

Table 2: PDF refinement results of diffraction data computed from energy-minimized Crystalline and spherical gold nanoparticle ensembles evaluated at 5 different wavelengths.

Nominal Size (Å)	λ (Å)	a (Å)	D (Å)	B_{iso} (Å²)	Rw	Δr (Å)	q_{min} (1/Å)	q_{max} (1/Å)
48.75	0.21	4.05594	44.20	0.044	0.097	0.10	1.56	27.6
97.50	0.21	4.06000	93.48	0.020	0.047	0.10	1.56	27.6
150	0.21	4.06190	145.91	0.011	0.036	0.10	1.56	27.6
195	0.21	4.06251	191.01	0.011	0.036	0.10	1.56	27.6
293	0.21	4.06264	289.61	0.003	0.017	0.10	1.56	27.6
48.75	0.56	4.05534	44.85	0.058	0.071	0.28	1.56	22.4
97.50	0.56	4.05988	93.72	0.029	0.036	0.28	1.56	22.4
150	0.56	4.06185	146.38	0.019	0.030	0.28	1.56	22.4
195	0.56	4.06248	191.56	0.012	0.020	0.28	1.56	22.4
293	0.56	4.06263	289.86	0.008	0.012	0.28	1.56	22.4
48.75	0.71	4.05452	45.97	0.081	0.067	0.35	1.54	17.7
97.50	0.71	4.05968	94.51	0.040	0.044	0.35	1.54	17.7
150	0.71	4.06179	147.47	0.025	0.038	0.35	1.54	17.7
195	0.71	4.06244	192.69	0.017	0.030	0.35	1.54	17.7
293	0.71	4.06261	291.16	0.010	0.023	0.35	1.54	17.7
48.75	1.00	4.05359	46.82	0.102	0.055	0.50	1.64	12.6
97.50	1.00	4.05947	95.33	0.057	0.034	0.50	1.64	12.6
150	1.00	4.06167	148.44	0.037	0.028	0.50	1.64	12.6
195	1.00	4.06238	193.58	0.025	0.021	0.50	1.64	12.6
293	1.00	4.06259	292.15	0.015	0.016	0.50	1.64	12.6
48.75	1.54	4.05291	47.72	0.155	0.053	0.77	1.70	8.2
97.50	1.54	4.05929	96.39	0.078	0.038	0.77	1.70	8.2
150	1.54	4.06158	149.48	0.049	0.030	0.77	1.70	8.2
195	1.54	4.06232	194.53	0.033	0.024	0.77	1.70	8.2
293	1.54	4.06257	293.08	0.002	0.020	0.77	1.70	8.2

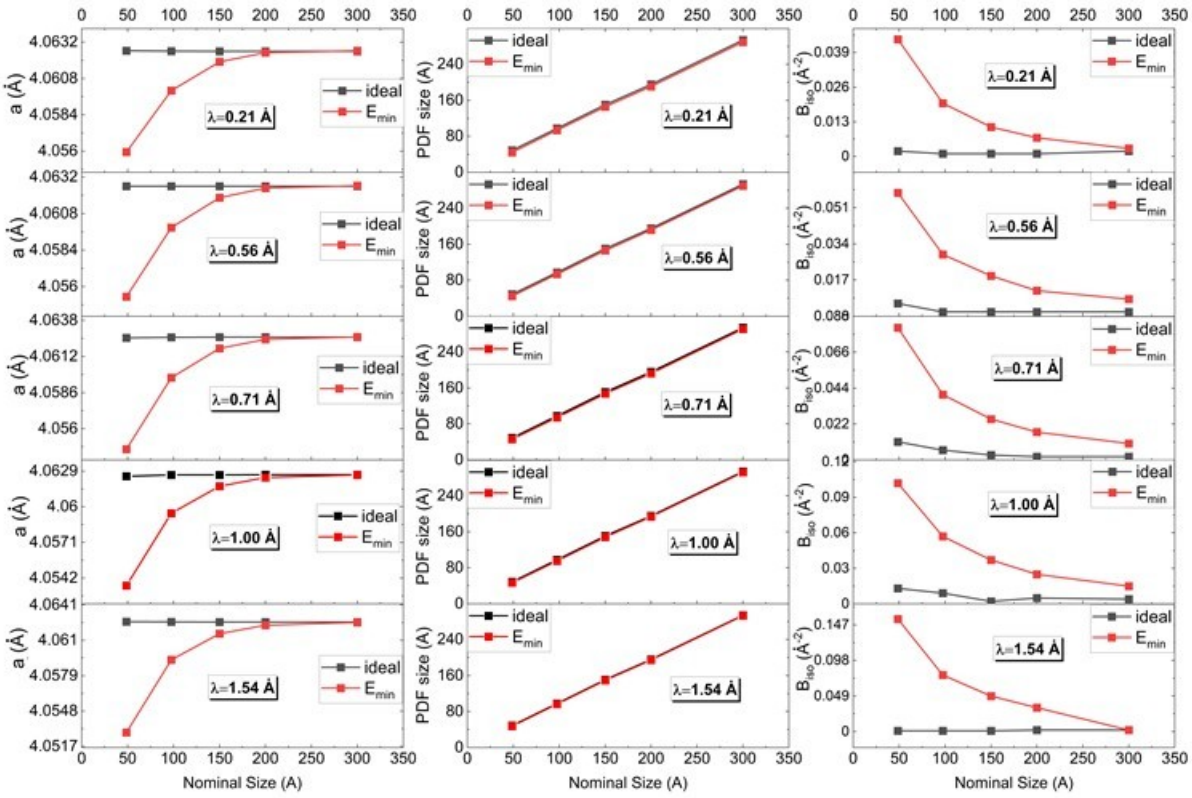

Figure 4: Left: Lattice parameters extracted from PDF refinement performed on simulated diffraction data of gold nanoparticle ensembles irradiated by five different wavelengths of X-rays. **Middle:** Refined average crystallite diameters from ideal-crystalline and energy-minimized nanoparticles. **Right:** Refined isotropic atomic displacement parameters B_{iso} from ideal-crystalline and energy-minimized nanoparticles.

Finally, when it comes to the extracted B_{iso} values, we notice that there is a significant increase in the refined values for energy-minimized nanoparticles compared with those of ideal nanocrystals. As explained in the beginning of this section, these increases could be the result of both static and dynamic atomic displacements if the refined diffraction data were experimentally obtained (12). In our case, however, we simulated the diffraction data based on the minimum-energy configurations of our nanocrystalline particles, where the energy-minimization algorithm ignored the zero-point vibrational movement of atoms (15, 23). As a result, the isotropic atomic displacement values extracted could only come from static displacements of atoms. Considering that the largest B_{iso} values obtained from the ideal-crystalline particle ensembles are around 0.013 Å^2, the B_{iso} values of energy-minimized nanoparticles that are in excess of 0.013 Å^2 could be interpreted as contributed from static displacements of atoms. These static displacements of atoms are maximized for the smallest nanoparticles and minimized for the largest ones (see the right column of Figure 4), in accordance with changes in the remaining structural parameters.

Evaluation of Refined Structural Parameters Against Real-Space Structural Parameters

In order to evaluate the accuracy of our refinement results, we also computed the average structural parameters of our nanoparticle ensembles based on individual atomic coordinates. These atomistic calculations were performed by classifying all atoms according to their coordination numbers. This was done by counting the first nearest neighbors of all atoms within spheres of 3.2 Å, radii centered at the positions of atoms. Those with a coordination number of 12 were considered core atoms, and the remaining ones were considered as surface layer atoms. Given the discrete atomic coordinates of a nanoparticle, the diameter distribution was calculated by surface atom coordinates. One diameter was calculated for each pair of surface atoms, provided that the line connecting these atoms crossed the center of the particle. This resulted in 525, 2205, 5359, 9105, and 20673 total numbers of diameters for 5, 10, 15, 20, and 30 nm particles, respectively. The minimum (D_{min}), maximum (D_{max}), average (D_{ave}), and standard deviation of these diameters for each particle are presented in Table 3. The last row reports the B_{iso} value for bulk gold, which was obtained by MD simulations using periodic boundary conditions in 3 dimensions and ignoring small size and surface effects formerly present in nanocrystalline gold particles.

Table 3: Structural parameters (average values and standard deviations) obtained from calculations based on atomic coordinates of energy-minimized gold nanoparticles. N_{surf}/N reports the ratio of the surface atoms' number to the total number of atoms in a single nanoparticle.

Nominal Size (Å)	$\frac{N_{surf}}{N}$	No. unit cell	a_{ave} (Å)	a_{std} (Å)	D_{min} (Å)	D_{max} (Å)	D_{ave} (Å)	D_{std} (Å)	B_{iso} (Å^2)
48.75	0.29	2539	4.0542	0.0256	43.43	48.23	45.89	1.4	0.026
97.50	0.15	24487	4.0588	0.0185	91.96	96.93	94.70	1.3	0.025
150	0.10	95396	4.0608	0.0145	144.82	149.87	147.59	1.4	0.022
195	0.078	213267	4.0618	0.0119	189.42	194.53	192.24	1.4	0.023
293	0.053	739799	4.0624	0.0087	286.95	292.05	289.73	1.4	N/A
Bulk	≈∞	≈∞	4.0626	≈0	N/A	N/A	N/A	N/A	0.019

The average lattice parameters of unit cells making up the energy-minimized nanoparticles were calculated by finite-strain theory. Here, all nanoparticles were decomposed into repeating unit cells, where a unit cell was constructed of one basis atom plus its 12 first-nearest neighbors. Under-coordinated surface atoms with a coordination number of less than 12 were eliminated from the calculation. To relate the average lattice parameters of the energy-minimized nanoparticles a_{ave} to that of the ideal crystalline nanoparticles a_0, we used $\varepsilon_{ave}=\frac{a_{ave}-a_0}{a_0}$, where a_0= 4.0626 Å and ε_{ave} is the average lattice strain (25). Next, ε_{ave} was calculated After that, F was obtained and E was computed, and the three eigenvectors of the symmetric tensor E specified the relative variation $\Delta a/a_0$ of the lattice by the following procedure: first, for each unit cell, a 3-by-3 deformation gradient F was computed by finding coordinate vectors connecting the basis atom to its first-nearest neighbor atoms in the reference structure, X_i, which were the ideal crystal coordinates in our case and in the deformed or energy-minimized structure, x_i, with i=1,2...12. Then F was determined by a least-squares fit following the method from the literature (26, 27):

$$FX_i \approx x_i \forall i=1\ldots12 \quad \text{(Eq.7)}$$

$$E=\frac{1}{2}\left(F^TF-I\right) \quad \text{(Eq.8)}$$

parameter in the principal directions of deformation. The mean strain ε_{ave} of all unit cells in the particle was then multiplied by a_0 to evaluate the average

lattice parameter a_{ave} of the energy-minimized nanoparticle. Table 3 presents the total number of unit cells considered for a given nanoparticle (column 3) along with the corresponding average lattice parameters and their standard deviations (4th and 5th columns, respectively). Finally, mean square displacements (MSD) of particles were calculated with LAMMPS without applying periodic boundary conditions to take into account the free surfaces of nanoparticles. Before each calculation, all particles were subjected to: **1)** heating up to 600 K within 50 ps; **2)** equilibration at 600 K for 50 ps; **3)** cooling back to 10K within 50 ps; and **4)** equilibration at 10 K for 100 ps in an NVT ensemble. MSD calculations were simulated at 10 K because molecular dynamics algorithms do not allow simulations at 0K. In the case of bulk gold, NPT ensemble was used instead of NVT to eliminate surface effects. After the equilibration step, a 1000 ps production run for MSD calculation was performed. We note that equilibration time significantly affects MSD. If the system is not equilibrated well, MSD is overestimated and contains high, time-dependent fluctuations. Thus, we increased the equilibration time at 10 K from 100 to 1000 and 2000 ps for 15 and 20 nm particles, respectively. However, we were not able to complete a full calculation for 30 nm particles in a reasonable time, so the corresponding B_{iso} for 30 nm particles was excluded from Table 3. Lastly, the isotropic atomic displacement parameter B_{iso} was calculated by $B_{iso}=8\pi^2 MSD$. These are presented in the last column of Table 3.

As shown, an increase in the nominal size of the nanoparticles results in a dramatic decrease in the $\frac{N_{surf}}{N}$ ratio, which directly influences the average lattice parameters obtained for the particles since the relative mobility of surface atoms compared to bulk atoms in a nanoparticle is significantly higher. Higher mobility of surface atoms, then, results in larger decreases in the average lattice parameters from 4.0626 Å. One may notice that the changes in a_{ave} are not as dramatic as those of $\frac{N_{surf}}{N}$ ratios; the reason for that lies in our computation method of a_{ave}. As described, we only considered atoms that had full coordination, i.e. had exactly 12 nearest-neighbors, to construct a unit cell. Therefore, the most mobile surface atoms are not considered in our average unit cell calculations, which disregard the largest inward movements of the outermost-surface atoms. Secondly, the average diameters obtained from the particles correlate well with the nominal sizes. Compared with the D_{ave} values of ideal crystalline nanoparticles, which are 46.10, 94.90, 147.70, 192.30, and 289.80 ± 1.5 Å, respectively, the D_{ave} of energy-minimized particles are smaller, but the difference is within the standard deviation of the diameter distributions (D_{std}). Hence, real space calculations do not indicate appreciable size changes due to energy-minimization, at least not with the calculation method described here. Finally, looking at B_{iso} values, we immediately see their inverse relationship with the nominal sizes of the nanoparticles. This is expected and can be explained with similar arguments as the lattice parameter changes. Higher surface atom ratios enable much larger atomic movements, and these immediately increase the MSD values. At the ultimate limit of a bulk structure, B_{iso} converges to 0.019 Å^2, which is the minimum of all others.

Next, we compared the values in Table 3 with the PDF refinement results of energy-minimized particles in Table 2. However, this is not trivial since we have 5 sets of refined parameters for each X-ray wavelength and large changes in parameter values are observed at different wavelengths. Consistent with past literature (12), we select the refinement results for 0.21 Å, as reference value of PDF refinement since it yields the highest real-space resolution and minimum Fourier truncation errors. Comparing Table 3 with Table 2, we observe that the lattice parameters computed atomistically are slightly lower than those from PDF refinement, although the differences are at the third decimal and are within the standard deviations reported in Table 3. Considering that the atomistic simulations do neglect under-coordinated atoms, the observed agreement is surprisingly good. When we switch to refined diameters, we realize that they correlate well with the average diameters calculated within their standard deviations. Among the three structural parameters, refined B_{iso} values are the most divergent from their atomistically-computed counterparts. Although their magnitude orders are similar, the dramatic size dependence of the refined B_{iso} values is not confirmed by atomistic calculations. One reason for explaining the disagreement is the Gaussian model of atomic displacements assumed by the PDF refinement algorithm. As confirmed indirectly by the changes in the lattice parameters and average diameters, the atoms within energy-minimized nanoparticles do not experience random displacements as implied by Gaussian models. Atomic displacements are uneven at different atomic layers of the particles, and their directions are mostly inward. Hence, the incompatibility between assumed models of atomic movements contributes to the divergences in the extracted B_{iso} values. Secondly, our Fourier truncation errors are expected to cause large errors in the refined atomic displacement values from PDF, as shown in previously (12), since even with the smallest X-ray wavelength, our q_{max} value is still less than the suggested 30 Å^{-1} limit. Thirdly, the B_{iso} values from the refinement of energy-minimized nanoparticles must be cleared from the minimum error limits for a fair comparison, even though Table 1 shows that their contribution is within 0.002 Å^2 for all sizes at $\lambda=0.21$ Å. Lastly, the refined B_{iso} values from PDF analysis are actually from the static

displacements of atoms, whereas our LAMMPS calculations consider hundreds of nanoparticle ensembles where only the dynamic atomic displacements are reported in the MSD calculations. This shows that even with error-free diffraction data, extracting atomic displacement parameters based on PDF analysis of X-ray diffraction data is a challenging task that requires carefully-planned data generation/collection strategies as well as compatible parameter definitions. Overall, the agreement between atomistic calculations and PDF-refined structural parameters of spherical gold nanoparticles is satisfactory.

CONCLUSIONS

In this study, we used atomistic calculations to generate and analyze ideal diffraction data from powders of spherical gold nanoparticles to evaluate the accuracy limits of Pair Distribution Function analysis in extracting the lattice parameter, average particle size, and atomic displacement values. Our results show that the minimum uncertainties in the extracted structural parameters from the diffraction data of ideal-crystalline nanoparticles are within ± 5 x 10^{-5} Å the average lattice parameter, which is the most stable structural parameter irrespective of the X-ray wavelength selected. The diameters obtained from PDF analysis are closer to the maximum values of the diameter distributions of ideal crystalline particles since PDF analysis relies on analytical models to obtain average crystal sizes from the approximate position of where the G(r) curve decays down to noise level. Still, the extracted sizes are within 1% of the nominal sizes. A high q_{max} value is desired for the highest resolution of crystallite size. Finally, B_{iso} values are bound within 0.013 $Å^2$ for the systems we studied, with higher uncertainties present for the smallest nanocrystals and lower ones for the largest nanocrystals. The size dependencies on B_{iso} uncertainties are consistent with the experimental observations of surface atom mobility and its effects on nanoparticles with small crystallite sizes.

PDF analyses of energy-minimized nanoparticles revealed consistent trends with similar analyses performed with crystallographic solution algorithms (11). Decreasing lattice parameters with decreasing nominal particle size is confirmed with all selected X-ray wavelengths, although the amount of decrease depends on the q_{max} range of the diffraction data. However, the inward movement of surface atoms resulting from the energy-minimization process was not captured by the PDF method when q_{max} was less than 15 $Å^{-1}$. This again confirms that PDF-based crystallite sizes are very sensitive to the wavelength selected. A significant increase in B_{iso} was observed as a result of the energy minimization for all particle sizes and for all X-ray wavelengths. The amount of enhancement was the most prominent for the smallest nanoparticles since they have the largest ratio of surface atoms.

Atomistic calculations of structural parameters from energy-minimized nanoparticles agree fairly well with those obtained by PDF analysis. The lattice parameters and average particle sizes agree within their standard deviations. However, we were not able to directly correlate the refined B_{iso} values with those from real-space calculations. Possible reasons were identified as incompatible definitions of mean square displacements of atoms in the two methods compared, and large Fourier truncation errors resulting from limited q_{max} range. These could be significant when q_{max} is less than 30 $Å^{-1}$, as reported previously (12).

To conclude, our results show that PDF analysis can be a strong tool for researchers who want to study the structural properties of nanocrystalline powders. The uncertainties in the refined parameters are quite low, even with less-than-ideal diffraction data and modest q_{max} values. Moreover, one can follow our proposed methodology to estimate the analysis errors for specific cases since our method is generalizable and uses open-source programs and optimized computation routines. However, we highlight that the estimated errors obtained from the proposed methodology would only yield the minimum expected uncertainties of structural parameters; when working with measured XRD data that contains undesirable scattering components such as photon counting and sampling statistics, size and/or lattice parameter distributions in the sample, background scattering, etc. the uncertainty to be expected must increase. Therefore, the accurate interpretation of X-ray diffraction data from nanocrystalline powders requires great care and meticulous analysis of different sources of error and their bounds.

CONFLICT OF INTEREST

The authors declare no conflicts of interest.

ACKNOWLEDGMENTS

We would like to thank Dr. İlknur Eruçar and Dr. Shangmin Xiong for helpful discussions and guidance on running molecular dynamics simulations of metallic nanocrystalline particles. This research used the resources of Özyeğin University High Performance Computing Center and was funded by the Scientific and Technological Research Council of Turkey (TÜBİTAK) under the BİDEB 2232 International Fellowship of Outstanding Researchers Program (Project no:118C268).

REFERENCES

1. Prasad N, Karthikeyan B. Tunable bandgap and blue emission of ZnS nanoparticles induced by controlled S

vacancies. Journal of Applied Physics. 2019 Feb 28;125(8):085702. <DOI>.

2. Tran N, Zhao W, Carlson F, Davidson JH, Stein A. Metal Nanoparticle–Carbon Matrix Composites with Tunable Melting Temperature as Phase-Change Materials for Thermal Energy Storage. ACS Appl Nano Mater. 2018 Apr 27;1(4):1894–903. <DOI>.

3. Ingham B. X-ray scattering characterisation of nanoparticles. Crystallography Reviews. 2015 Oct 2;21(4):229–303. <DOI>.

4. Kang S-JL, Park J-H, Ko S-Y, Lee H-Y. Solid-State Conversion of Single Crystals: The Principle and the State-of-the-Art. Green DJ, editor. J Am Ceram Soc. 2015 Feb;98(2):347–60. <DOI>.

5. Neder RB, Proffen T. Exact and fast calculation of the X-ray pair distribution function. J Appl Crystallogr. 2020 Jun 1;53(3):710–21. <DOI>.

6. Rietveld HM. A profile refinement method for nuclear and magnetic structures. J Appl Crystallogr. 1969 Jun 2;2(2):65–71. <DOI>.

7. Juhás P, Farrow CL, Yang X, Knox KR, Billinge SJL. Complex modeling: a strategy and software program for combining multiple information sources to solve ill posed structure and nanostructure inverse problems. Acta Crystallogr A Found Adv. 2015 Nov 1;71(6):562–8. <DOI>.

8. Petkov V, Bedford N, Knecht MR, Weir MG, Crooks RM, Tang W, et al. Periodicity and Atomic Ordering in Nanosized Particles of Crystals. J Phys Chem C. 2008 Jun 1;112(24):8907–11. <DOI>.

9. Popa NC, Balzar D. Size-broadening anisotropy in whole powder pattern fitting. Application to zinc oxide and interpretation of the apparent crystallites in terms of physical models. J Appl Crystallogr. 2008 Jun 1;41(3):615–27. <DOI>.

10. Bugaev AL, Guda AA, Lomachenko KA, Shapovalov VV, Lazzarini A, Vitillo JG, et al. Core–Shell Structure of Palladium Hydride Nanoparticles Revealed by Combined X-ray Absorption Spectroscopy and X-ray Diffraction. J Phys Chem C. 2017 Aug 24;121(33):18202–13. <DOI>.

11. Xiong S, Öztürk H, Lee S-Y, Mooney PM, Noyan IC. The nanodiffraction problem. J Appl Crystallogr. 2018 Aug 1;51(4):1102–15. <DOI>.

12. Toby BH, Egami T. Accuracy of pair distribution function analysis applied to crystalline and non-crystalline materials. Acta Crystallogr A Found Crystallogr. 1992 May 1;48(3):336–46. <DOI>.

13. Farrow CL, Billinge SJL. Relationship between the atomic pair distribution function and small-angle scattering: implications for modeling of nanoparticles. Acta Crystallogr A Found Crystallogr. 2009 May 1;65(3):232–9. <DOI>.

14. Plimpton S. Fast Parallel Algorithms for Short-Range Molecular Dynamics. Journal of Computational Physics. 1995 Mar;117(1):1–19. <DOI>.

15. Sheng HW, Kramer MJ, Cadien A, Fujita T, Chen MW. Highly optimized embedded-atom-method potentials for fourteen fcc metals. Phys Rev B. 2011 Apr 20;83(13):134118. <DOI>.

16. Öztürk H, Yan H, Hill JP, Noyan IC. Sampling statistics of diffraction from nanoparticle powder aggregates. J Appl Crystallogr. 2014 Jun 1;47(3):1016–25. <DOI>.

17. Debye P. Zerstreuung von Röntgenstrahlen. Ann Phys. 1915;351(6):809–23. <DOI>.

18. Warren BE. X-ray diffraction. Dover ed. New York: Dover Publications; 1990. 381 p. ISBN: 978-0-486-66317-3.

19. Juhás P, Davis T, Farrow CL, Billinge SJL. *PDFgetX3* : a rapid and highly automatable program for processing powder diffraction data into total scattering pair distribution functions. J Appl Crystallogr. 2013 Apr 1;46(2):560–6. <DOI>.

20. Trueblood KN, Bürgi HB, Burzlaff H, Dunitz JD, Gramaccioli CM, Schulz HH, et al. Atomic Dispacement Parameter Nomenclature. Report of a Subcommittee on Atomic Displacement Parameter Nomenclature. Acta Crystallogr A Found Crystallogr. 1996 Sep 1;52(5):770–81. <DOI>.

21. Dippel A-C, Roelsgaard M, Boettger U, Schneller T, Gutowski O, Ruett U. Local atomic structure of thin and ultrathin films *via* rapid high-energy X-ray total scattering at grazing incidence. IUCrJ. 2019 Mar 1;6(2):290–8. <DOI>.

22. Gilbert B. Finite size effects on the real-space pair distribution function of nanoparticles. J Appl Crystallogr. 2008 Jun 1;41(3):554–62. <DOI>.

23. Guinier A. X-Ray Diffraction: In Crystals, Imperfect Crystals, and Amorphous Bodies. Dover Publications, Mineola, NY, USA; 2013. ISBN: 978-0-486-68011-8.

24. Huang WJ, Sun R, Tao J, Menard LD, Nuzzo RG, Zuo JM. Coordination-dependent surface atomic contraction in nanocrystals revealed by coherent diffraction. Nature Mater. 2008 Apr;7(4):308–13. <DOI>.

25. Xiong S, Lee S-Y, Noyan IC. Average and local strain fields in nanocrystals. J Appl Crystallogr. 2019 Apr 1;52(2):262–73. <DOI>.

26. Li group. Least-Square Atomic Strain [Internet]. 2005. <URL>.

27. Stukowski A, Markmann J, Weissmüller J, Albe K. Atomistic origin of microstrain broadening in diffraction data of nanocrystalline solids. Acta Materialia. 2009 Mar;57(5):1648–54. ISBN: 978-0-486-68011-8.

Accuracy Limits of Pair Distribution Function Analysis in Structural Characterization of Nanocrystalline Powders by X-ray Diffraction

Abolfazl Baloochiyan[1], Merdan Batyrow[1], Hande Öztürk[1*]

[1]Özyeğin University, Department of Mechanical Engineering, İstanbul, 34794, Turkey

SUPPORTING INFORMATION

Additional details of our Molecular Dynamics (MD) simulations are provided in this section.

Force-field selection:
For MD simulations, interatomic forces were modeled with optimized embedded atom method (EAM) developed by Sheng et al. (2011) [**15**] and available online to be used with LAMMPS [**14**]. The force-field was highly optimized to match the experimental database and has been shown to have validity in the modeling of gold nanoparticles by Xiong et al. (2018) [**11**].

MD steps and results:
Before starting the MD simulations with LAMMPS, five separate spherical gold nanocrystal models with diameters of 5, 10, 15, 20, and 30 nm were generated from an FCC lattice with 4.0626 Å lattice parameter. This corresponded to the bulk lattice parameter of gold at 0 K calculated with the selected force-field. Generated nanocrystals were each placed in the center of a simulation box. The volume of the simulation box and the number of atoms in each nanocrystal are given in **Table S1**. An example of a 10 nm nanocrystal inside a simulation box is shown in **Figure S1**. Afterwards, MD simulations were performed with non-periodic boundary conditions applied in all directions since we were studying colloidal, free-standing gold nanocrystals. We followed six steps in the simulations, as shown in **Table S2**. They are as follows:

1) The energy minimization was performed with the force and energy change ratio criteria of 10^{-6} eV Å^{-1} and 10^{-6}, respectively, for convergence within a maximum of 80 ps. Final atomic configuration obtained from this step was assumed to be energy-minimized at 0 K and was used in subsequent Pair Distribution Function analyses. The steps below were used for MSD (Mean Square Displacement) calculations.

2-4) Following energy minimization, an annealing simulation cycle was performed between 10-600 K in NVT ensemble by raising the temperature of the system and cooling it back. This step is important since it allows atoms to overcome their energy barriers and avoid local minimum energy configurations [**25**]. Total simulation length of this step was 150 ps.

5) Then, the system was equilibrated at 10 K temperature before MSD calculation. This step makes sure that system is energetically equilibrated at given conditions and results in reliable data out of MD. With respect to time, the temperature and energy change of the system, during annealing and equilibration, are shown in **Figures S2A** and **S2B**. Total simulation length of this step was 100 ps.

6) Finally, a production run was performed to calculate the MSD of the systems during the 1000 ps simulation as shown in **Figure S2C**.

Table S1 : The number of atoms and the volume of the simulation boxes used in MD runs of each nanocrystal

Size (nm)	Number of atoms	MD box volume (nm^3)
5	3589	324.81
10	28897	1622.23
15	106114	4947.76
20	231477	9938.38
30	781145	30371.33

Table S2 : MD steps with simulation parameters.

Step	Ensemble	Temperature (K)	Simulation time (ps)	Timestep (ps)	Note
1	-	0	80*	0.001	Energy minimization
2	NVT**	2 – 600	50		Annealing simulation
3		600	50		
4		600 - 10	50		
5		10	100		Equilibration run
6		10	1000		Production run – MSD calculation

* Specified time is the maximum allowed simulation time in case the given energy and force convergence criteria are not satisified .
** In case of bulk system NPT ensemble is used.

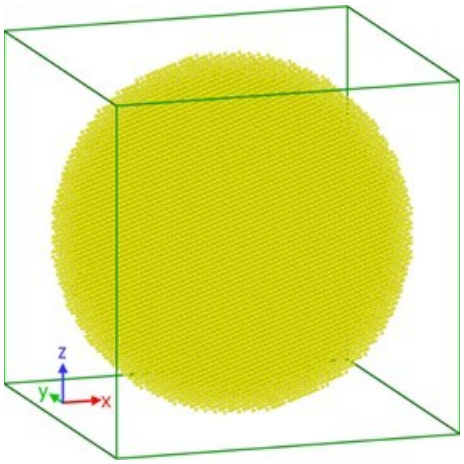

Figure S1: 10 nm diameter spherical gold nanocrystal model is shown inside its simulation box.

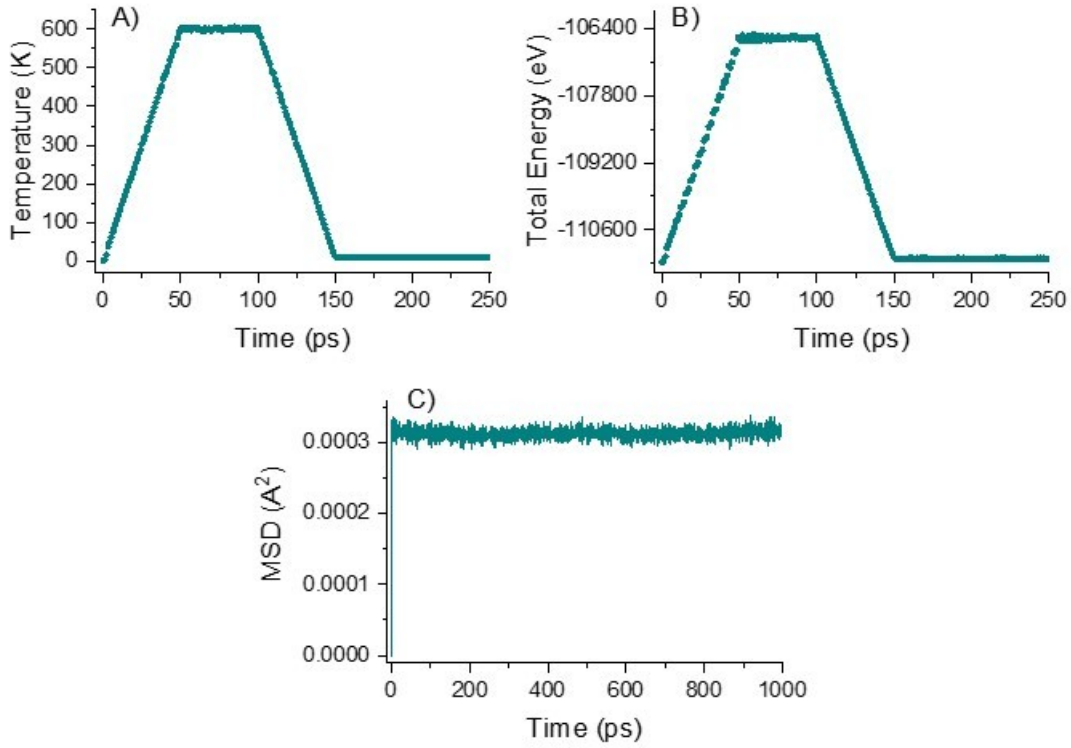

Figure S2: **A)** Temperature vs. time**, B)** Total energy vs. time, and **C)** MSD vs. time for 10 nm gold nanocrystal model.